iScience

CellPress
OPEN ACCESS

Article

Matching the Directions of Electric Fields from Triboelectric and Ferroelectric Charges in Nanogenerator Devices for Boosted Performance

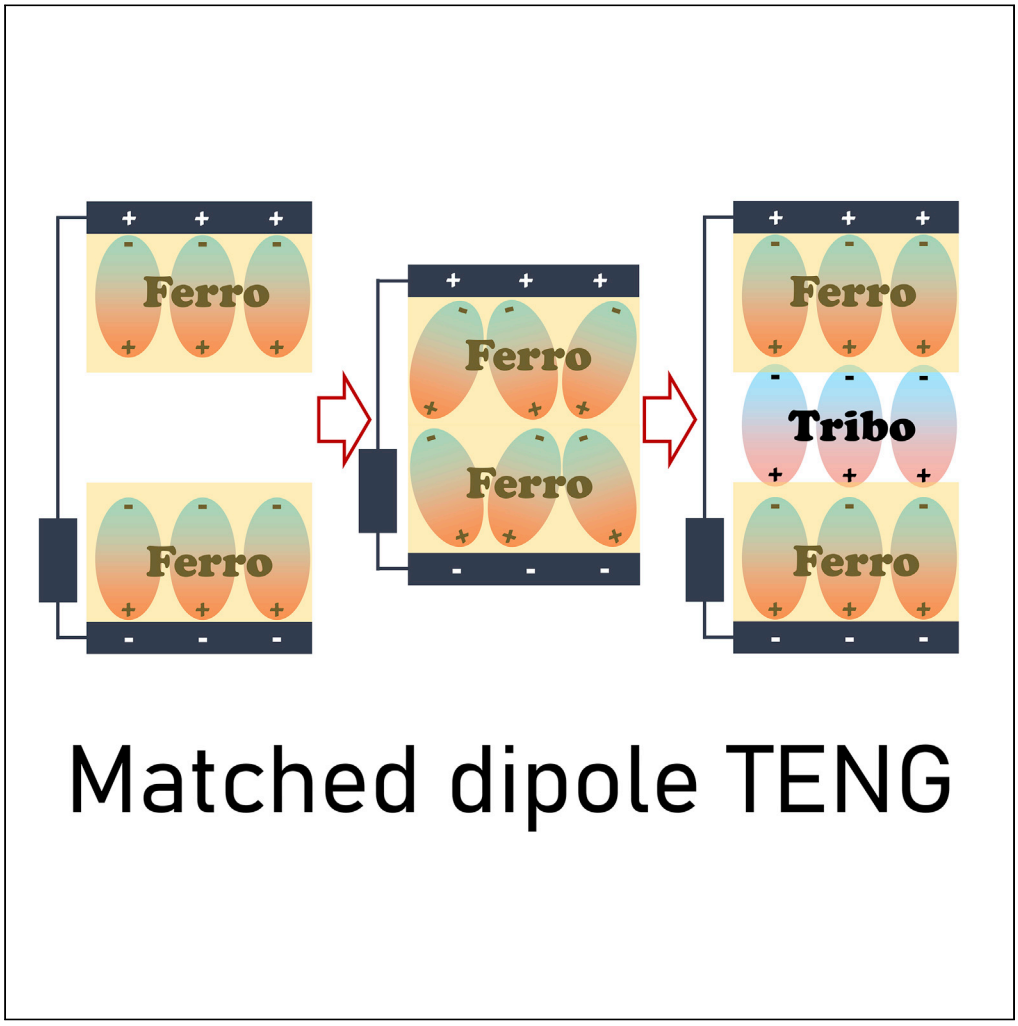

Andris Šutka,
Kaspars Mālnieks,
Linards Lapčinskis,
Martin Timusk,
Kaspars Pudzs,
Martins Rutkis

andris.sutka@rtu.lv

HIGHLIGHTS

TENG devices based on ferroelectric polymer/$BaTiO_3$ composites were prepared

$\vec{E}$ from ferroelectric dipoles and triboelectric charges drive electrostatic induction

Matching $\vec{E}$ directions in TENG device lead to up to four times higher performance

$\vec{E}$ from different sources are summing up and provide a stronger induction

Šutka et al., iScience *23*, 101011
April 24, 2020
https://doi.org/10.1016/j.isci.2020.101011

iScience

CellPress
OPEN ACCESS

Article

Matching the Directions of Electric Fields from Triboelectric and Ferroelectric Charges in Nanogenerator Devices for Boosted Performance

Andris Šutka,[1,5,*] Kaspars Mālnieks,[1] Linards Lapčinskis,[2] Martin Timusk,[3] Kaspars Pudzs,[4] and Martins Rutkis[4]

SUMMARY

Embedding additional ferroelectric dipoles in contacting polymer layers is known to enhance the performance of triboelectricnanogenerator (TENG) devices. However, the influence of dipoles formed between the triboelectric surface charges on two contacting ferroelectric films has been ignored in all relevant studies. We demonstrate that proper attention to the alignment of the distinct dipoles present between two contacting surfaces and in composite polymer/$BaTiO_3$ ferroelectric films can lead to up to four times higher energy and power density output compared with cases when dipole arrangement is mismatched. For example, TENG device based on PVAc/$BaTiO_3$ shows energy density increase from 32.4 $\mu J\ m^{-2}$ to 132.9 $\mu J\ m^{-2}$ when comparing devices with matched and mismatched dipoles. The presented strategy and understanding of resulting stronger electrostatic induction in the contacting layers enable the development of TENG devices with greatly enhanced properties.

INTRODUCTION

The field related to triboelectricnanogenerator (TENG) devices is emerging rapidly. Many original and creative TENG concepts have been presented in the literature for harvesting mechanical energy and converting it into electricity (Lee et al., 2019). The working principle of TENG devices is straightforward. The triboelectric materials (most commonly polymer insulators) are deposited on two conductive electrodes connected by an external circuit. Upon contacting-separating or sliding, surface charges are formed on the triboelectric materials, which induce an electrostatic charge on the conductive electrodes. Due to electrode oscillation or movement, a potential difference is created, which causes a current flow in the external electric circuit. TENG devices can be integrated into fabrics (Zhou et al., 2014), wearables (Kanik et al., 2015), interior objects (Dhakar et al., 2016), membranes (to harvest energy from sound) (Fan et al., 2015), and even implantable devices (Yao et al., 2018).

To enhance the performance of TENG, different approaches have been used. The most obvious way is to increase the specific contact area via nanostructuring (Zhang et al., 2015; Dudem et al., 2015; Zheng et al., 2014). Another possibility is the modification of surface or physicochemical properties of the triboelectric material (Šutka et al., 2019; Šutka et al., 2019; Lapčinskis et al., 2019; Fan et al., 2014; Yun et al., 2015; Wang et al., 2016). The performance can be also enhanced by using ferroelectric polymer or composite films as the contacting surfaces (Bai et al., 2014; Seung et al., 2017; Suo et al., 2016; Chun et al., 2015; Yang and Daoud, 2017; Choi et al., 2017; Lee et al., 2016; Šutka et al., 2018; Lapčinskis et al., 2019; Kim et al., 2019; Huang et al., 2020). State-of-the-art performance of ferroelectric material-based TENG devices can be expected when the ferroelectric material layers on contacting sides of the device are inversely polarized (Šutka et al., 2018; Lapčinskis et al., 2019). The contacted inversely polarized layers then act similarly to a series of connected capacitors (Lapčinskis et al., 2019). The total capacitance of the system decreases dramatically, whereas the potential difference increases as the air gap is created during separation. The induced charge redistribution in the external circuit manifests itself as current.

However, previous works related to TENG devices based on ferroelectric materials overlook the dipole that forms between the triboelectric surface charges on contacting surfaces. As soon as we consider this additional factor, it follows that the electric field direction from ferroelectric dipoles should match the direction of the electric field from triboelectric surface charge to achieve maximum electric field strength and

[1]Research Laboratory of Functional Materials Technologies, Faculty of Materials Science and Applied Chemistry, Riga Technical University, Paula Valdena 3/7, 1048 Riga, Latvia

[2]Institute of Technical Physics, Faculty of Materials Science and Applied Chemistry, Riga Technical University, Paula Valdena 3/7, 1048 Riga, Latvia

[3]Institute of Physics, University of Tartu, W. Ostwaldi Str. 1, 50411 Tartu, Estonia

[4]Laboratory of Organic Materials, Institute of Solid State Physics, Kengaraga 8, 1063 Riga, Latvia

[5]Lead Contact

*Correspondence: andris.sutka@rtu.lv

https://doi.org/10.1016/j.isci.2020.101011

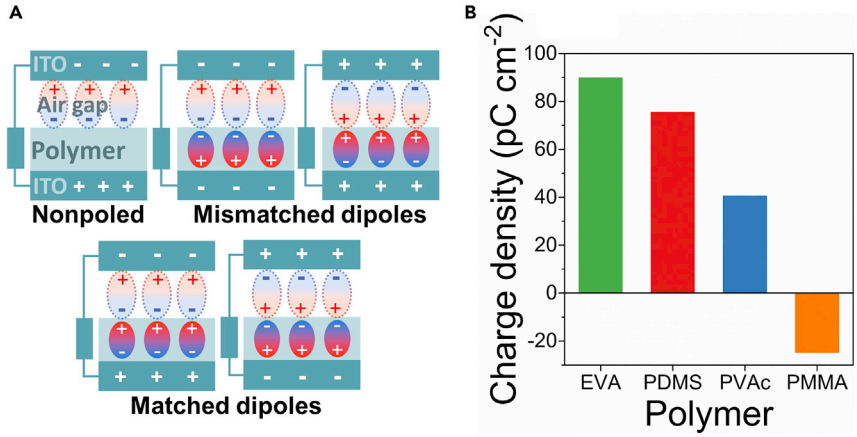

Figure 1. Dipole Formed between Polymer and ITO Can Be Matched with Ferroelectric Dipole

Schematic representation of possible interactions between surface charge dipoles in the air gap and ferroelectric dipoles in TENG device (A). The calculated surface charge density of non-ferroelectric polymers indicates the magnitude and direction of the formed dipole in contact-separation cycle (B) (See also Figures S7 and S8).

electrostatic induction. In other words, the alignment direction of ferroelectric dipoles has to coincide with the dipoles forming between the opposite charges on contacting surfaces as demonstrated in Figure 1A. In the present paper, we examine the performance of TENG devices when the electric field direction from surface charges and ferroelectric dipoles are matched or mismatched. To impart the ferroelectric properties for non-ferroelectric polymers used as triboelectric contacting layers, we added $BaTiO_3$ nanoparticles. $BaTiO_3$ were chosen as a feasible filler to allow preparation of ferroelectric polymer composite films so that contributions from contact-charging and ferroelectric dipoles could be compared. We demonstrate that matching the distinct kinds of dipoles present in TENG device leads to a significant increase in the power and energy density.

RESULTS AND DISCUSSION

Polydimethylsiloxane (PDMS), ethylene-vinyl acetate copolymer (EVA), poly(vinyl acetate) (PVAc), and poly(methyl methacrylate) (PMMA) were used in our studies to prepare TENG devices. The polymer films were spin coated on indium tin oxide (ITO) conductive electrode and contacted against another ITO (see Figure S1 for schematic TENG device representation). The polymer films were given ferroelectric properties by adding 7.5 vol% $BaTiO_3$ nanoparticles <100 nm in size (see Figure S2 for scanning electron microscopy (SEM) image). Particles were well dispersed throughout the polymer matrix in the prepared composites (the SEM images of cross-sections for different composites are demonstrated inFigures S3–S6). The experimental details for sample preparation are provided in SI.

The sign of triboelectric surface charges formed on pure polymers after contacting against ITO was determined by measuring the current between the underlying electrode and the ground in Faraday cup mode Figure 1B (see also Figure S7). Polymers PDMS, PVAc, and EVA obtain a negative charge on their surface, whereas for PMMA a positive charge is observed when contacted ITO. The sign of the net triboelectric charge did not change when $BaTiO_3$ nanoparticles were incorporated into the polymers (Figure S8).

All poled $BaTiO_3$/polymer composites exhibit piezoelectric properties (Figure S9). The poling procedure is described in Supplemental Information. The piezoelectric charges of 2.9 pC cm^{-2}, 10.9 pC cm^{-2}, 3.7 pC cm^{-2}, and 2.4 pC cm^{-2} were measured for $BaTiO_3$/EVA, $BaTiO_3$/PDMS, $BaTiO_3$/PVAc, and $BaTiO_3$/PMMA composites, respectively. The higher piezoelectric response of $BaTiO_3$/PDMS could be attributed to its larger deformability under the constant loading force. The elastic modulus values of the four polymers are 5.48 GPa for PMMA, 5.24 GPa for PVAc, 44.3 MPa for EVA, and 2.9 MPa for PDMS (Šutka et al., 2019).

Figure 2 shows time-resolved current (I_{SC}) and voltage measurements (V_{OC} at 1 GΩ) for TENG devices based on polymer composite layers and ITO. Composite layer in each of these TENG devices was tested as non-poled and also positively and negatively poled, so that ferroelectric dipole is matched and

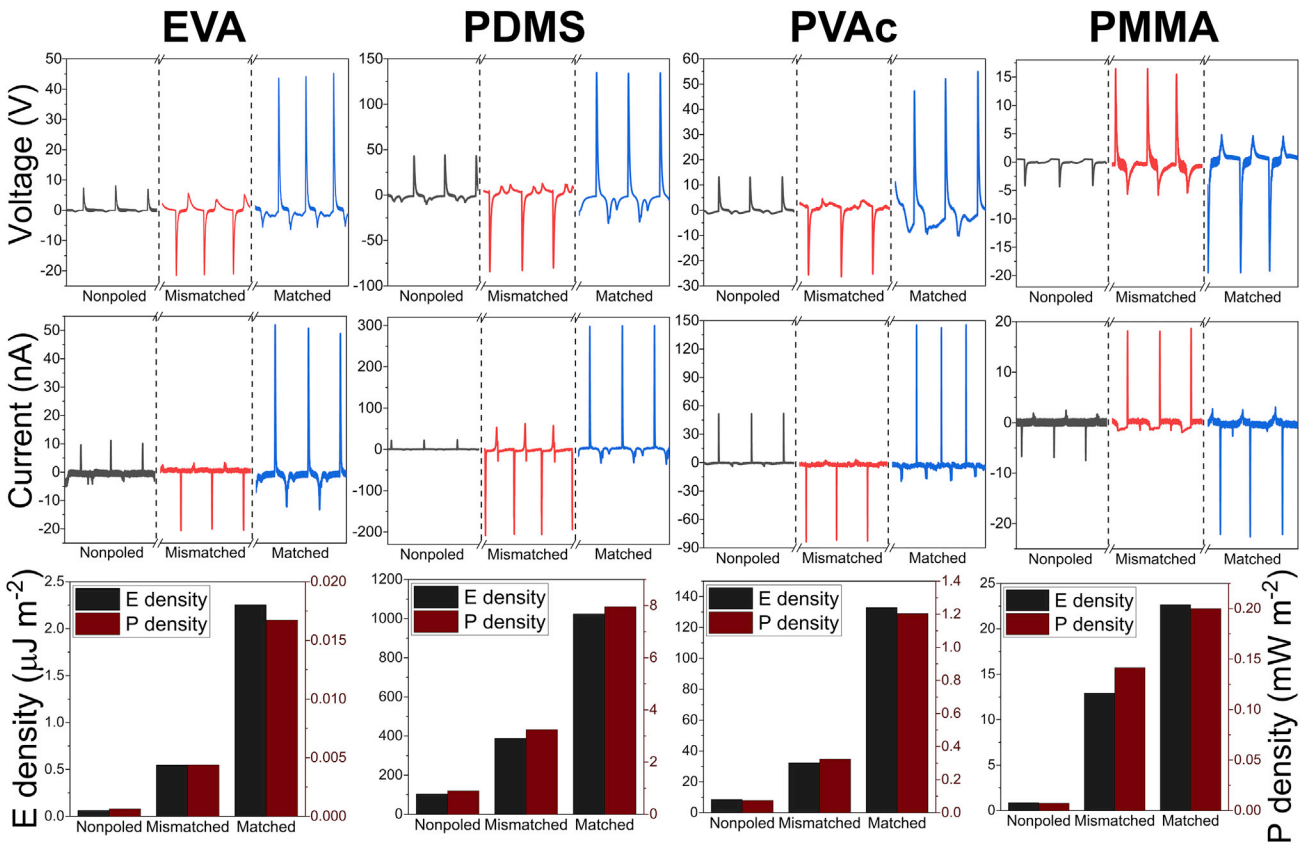

Figure 2. Comparison of Three Possible Dipole Alignment Configurations

Ferroelectric dipoles are not present (non-poled), they are mismatched to dipoles formed by contact electrification (mismatched), and they are matched in the same direction as contact-electrification generated dipoles (matched). These states are shown to influence open-circuit voltage, short-circuit current, energy density, and power density for each $BaTiO_3$/polymer composite studied in this work.

mismatched with the previously determined surface charge. The performance of a TENG device is very different depending on whether a positive or negative voltage is applied for poling (Figure 2), regardless of the polymer used. This phenomenon of one polarization direction resulting in a larger impact than the other is widely reported before (Bai et al., 2014; Suo et al., 2016; Lee et al., 2016; Šutka et al., 2018; Lapčinskis et al., 2019; Kim et al., 2019; Huang et al., 2020); however, the explanation provided for that has been inaccurate. We argue that the observed difference can be explained by elementary match and mismatch between the directions of the electric field from the ferroelectric dipole moment and the dipole moment created by triboelectric charges. As we can see from Figure 2, for PVAc, EVA, and PDMS, which obtain a negative triboelectric surface charge after contacting ITO, better performance is observed when the positive pole of the ferroelectric dipole is facing away from the underlying ITO electrode. In the case of PMMA, which has a positive triboelectric surface charge after contacting ITO, better performance is observed when the negative pole of the ferroelectric dipole is facing away from the substrate ITO electrode. Net dipole direction between surface triboelectric charges was confirmed by COMSOL finite element simulation (Figure S10). The experiments show that the TENG device has higher performance when the direction of dipole between triboelectric surface charge and ferroelectric dipoles are matching.

To provide even more evidence, we constructed a TENG device where both ITO electrodes are covered with a $BaTiO_3$/polymer composite film. For the highest performance, the dipoles in the two films are polarized inversely (Šutka et al., 2018; Lapčinskis et al., 2019), whereas the polymer matrix material for each side is chosen so that the dipole moment direction of triboelectric and ferroelectric charges are matched. The surface charges on the contacted polymers used in the study were determined experimentally by measuring current in Faraday cup mode (Figure S11). A TENG device was constructed from PMMA and PDMS as

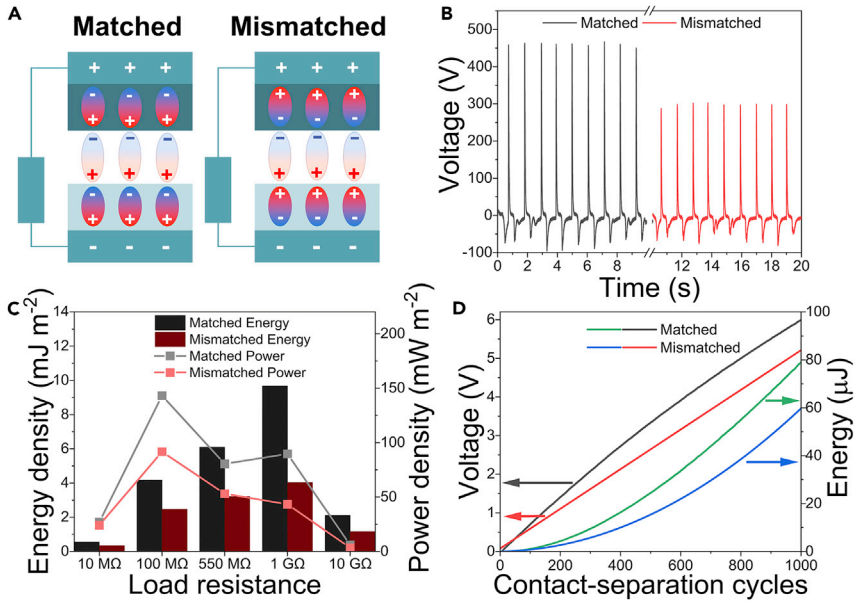

Figure 3. Comparison of TENG Devices Using Matched and Mismatched Dipole Configurations

Inversely polarized $BaTiO_3$/PDMS (top layer) and $BaTiO_3$/PMMA (bottom layer) TENG device constructed in a way that ferroelectric polarization direction is matched (left) and mismatched (right) with contact-electrification-generated surface charge dipole direction (A). Graphs for matched and mismatched configuration show V_{OC} (at 1 GΩ) (B), energy, and power density during one contact-separation cycle (C) and the voltage across 4.4 μF capacitor during charging with the corresponding stored energy (D) (see also Figures S11–S13).

PMMA charges positively and PDMS negatively. The poling direction in composite $BaTiO_3$/PMMA was chosen so that the negative pole of the ferroelectric dipole was facing away from the substrate, whereas $BaTiO_3$/PDMS was polarized so that the positive pole of ferroelectric dipole is facing away from the substrate. A schematic representation of the device is shown in Figure 3A. As expected, this particular TENG device performed excellently, and the output was superior to any other presented in this study. The peak open-circuit voltage (V_{OC}) of device with matched dipoles reached 460 V as shown in voltage-time plot in Figure 3B. The instant energy and power densities of this TENG device reached 9.7 mJ m^{-2} and 143.2 mW m^{-2}, respectively (black bars and gray line in Figure 3C). For comparison, a TENG device from the same polymers without $BaTiO_3$ NPs shows V_{OC} as small as 16 V and three orders of magnitude smaller energy and power densities of 0.012 mJ m^{-2} and 0.104 mW m^{-2} (Figure S12). Also, the TENG device from the same inversely polarized composite films but with mismatched dipoles exhibited significantly lower output—V_{OC} of 300 V (red line in Figure 3B) and instant energy and power densities of 4.0 mJ m^{-2} and 91.6 mW m^{-2} from the same contacting area (red bars and red line in Figure 3C).

We also performed a macroscale scanning Kelvin Probe measurements (detailed description given in Transparent Methodssection). The average surface potential for nonpolarized $BaTiO_3$/PDMS was determined to be 0.06 V. The average potential after contacting with PMMA was measured to be 146.4 V (surface potential maps of a nonpolarized sample before and after contacting PMMA are shown in Figure 4). Surface potential scanning was also performed on both positively and negatively polarized $BaTiO_3$/PDMS samples before and after contacting with PMMA. Average potential values at first were measured to be 24.3 V and −70.5 V, respectively. A quasi-permanent surface potential is created by ferroelectric dipoles in PDMS/$BaTiO_3$ composite layer. Just like in the case of a nonpolarized sample, contacting PMMA caused both samples to obtain an additional positive charge. Therefore, the average potential value grew to 107.2 V for the positively polarized sample and to −1.1 V in the case of the negatively polarized sample after they were contact separated. Full-surface potential maps for both polarized samples before and after the contact with PMMA are shown in Figure 4. Experimental results confirm the proposed mechanism for better performance of TENG devices where two sources of the electric field are present—triboelectric charges and ferroelectric dipoles. In the case of the matched direction of electric fields arising from triboelectric and ferroelectric dipoles, the electric field strength summarizes and amplifies the electrostatic induction

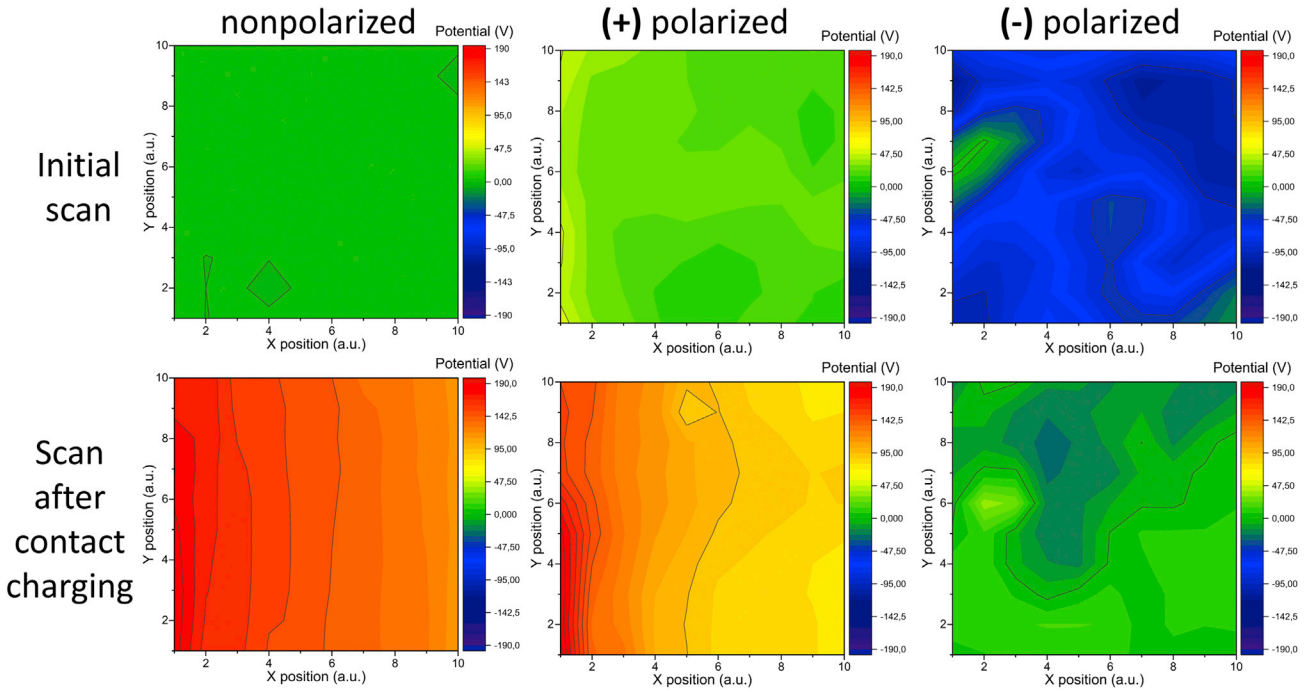

Figure 4. Surface Potential Maps of Three $BaTiO_3$/PDMS Composites (Nonpolarized, Positively and Negatively Polarized)

Top maps show respectively neutral, positive, and negative surface potential at initial scan. All surfaces show tendency to charge positively after contact with PMMA as evidenced by more positive surface potential (bottom). A gradual decrease of potential in the direction from left to right is observed because the triboelectric charge decreases as the surface is being scanned in this direction.

on TENG electrodes. Due to the potential difference between positive and negative induced charge, the stronger current flow between two TENG electrodes is measured. As shown in Figure S11B, a PDMS contact layer induces a positive current peak on the underlying electrode when contacted against PMMA. Therefore, surface potential of positively polarized PDMS layer (positive pole of ferroelectric dipole facing away from underlying electrode) after contact with PMMA corresponds to a matched dipole case, whereas the negatively polarized corresponds to mismatched dipoles.

The TENG device that was constructed from inversely polarized $BaTiO_3$/PDMS and $BaTiO_3$/PMMA composite films with matched dipoles was used to charge a 4.4 μF capacitor (Figure S13). This experiment is beneficial to understanding the practicality of the developed device because charged capacitors can be further used to charge batteries or power small sensors, and voltage across the capacitor also conveniently shows the amount of stored energy. By performing 1,000 contact-separation cycles the voltage across the capacitor increased by 6.0 V that corresponds to the stored energy of 79 μJ, as demonstrated in Figure 3D. In the meantime, TENG device constructed from equivalent contact layers, but with intentionally mismatched dipoles, increased the voltage across the capacitor only by 5.2 V and accumulated 60 μJ energy under the same operating conditions and number of contact-separating cycles.

The proof-of-concept demonstrated here can be further used to construct TENG devices with record performance. Polymers with a superior tendency for triboelectrification (Lapčinskis et al., 2019) and polymer composite materials with high intrinsic piezoelectric responses have been reported in literature widely (Zhang et al., 2018; Jeong et al., 2019; Han et al., 2019). A combination of methodology shown in this paper with high-performance ferroelectric materials could bring the TENG research community closer to new cutting-edge discoveries.

Conclusions

Results presented here shine a light upon the path to improvements in the construction of advanced TENG devices. The energy and power density of a TENG device can be increased up to four times by matching the

directions of electric fields arising from ferroelectric dipoles and triboelectric surface charges when compared with mismatched case. Matching of the dipoles magnifies the electric field strength and electrostatic induction on a conductive electrode that in turn leads to a higher voltage output.

Limitations of the Study

Performance values (V_{OC}, I_{SC}, Energy, and power density) in this work do not reach state-of-the-art level reported in the latest works. However, this study shows proof of concept that would allow to supersede all reported TENG devices. This could be done by more elaborate choice of polymer materials with superior contact-charging capabilities and by choosing ferroelectric materials with much higher piezoelectric constant d_{33}.

METHODS

All methods can be found in the accompanying Transparent Methods supplemental file.

DATA AND CODE AVAILABILITY

Supplemental Information can be found online.

SUPPLEMENTAL INFORMATION

Supplemental Information can be found online at https://doi.org/10.1016/j.isci.2020.101011.

ACKNOWLEDGMENTS

This research was supported by Riga Technical University's Doctoral Grant program. This research was also supported by the European Regional Development Fund within the project ''Hybrid energy harvesting systems'' 1.1.1.1./16/A/013.

AUTHOR CONTRIBUTIONS

K.M. and L.L. prepared the samples and conducted the experiments; K.P. performed Kelvin Probe measurements; M.R. contributed to interpretation of results; M.T. prepared COMSOL finite element simulation; A.Š. generated the main idea presented in the paper, designed the experiments, and wrote the paper with contributions from K.M. and L.L.

DECLARATION OF INTERESTS

The authors declare no competing interests.

Received: February 11, 2020
Revised: March 7, 2020
Accepted: March 19, 2020
Published: April 24, 2020

REFERENCES

Bai, P., Zhu, G., Zhou, Y.S., Wang, S., Ma, J., Zhang, G., and Wang, Z.L. (2014). Dipole-moment-induced effect on contact electrification for triboelectricnanogenerators. Nano Res. *7*, 990–997.

Choi, Y.S., Jing, Q., Datta, A., Boughey, C., and Kar-Narayan, S.A. (2017). A triboelectric generator based on self-poled Nylon-11 nanowires fabricated by gas-flow assisted template wetting. Energy Environ. Sci. *10*, 2180–2189.

Chun, J., Kim, J.W., Jung, W.S., Kang, C.Y., Kim, S.W., Wang, Z.L., and Baik, J.M. (2015). Mesoporous pores impregnated with Au nanoparticles as effective dielectrics for enhancing triboelectricnanogenerator performance in harsh environments. Energy Environ. Sci. *8*, 3006–3012.

Dhakar, L., Gudla, S., Shan, X., Wang, Z., Tay, F.E.H., Heng, C.-H., and Lee, C. (2016). Large scale triboelectricnanogenerator and self-powered pressure sensor array using low cost roll-to-roll UV embossing. Sci. Rep. *6*, 22253.

Dudem, B., Ko, Y.H., Leem, J.W., Lee, S.H., and Yu, J.S. (2015). Highly transparent and flexible triboelectricnanogenerators with subwavelength-architecturedpolydimethylsiloxane by a nanoporousanodic aluminum oxide template. ACS Appl. Mater. Interfaces *7*, 20520–20529.

Fan, F.R., Luo, J., Tang, W., Li, C., Zhang, C., Tian, Z., and Wang, Z.L. (2014). Highly transparent and flexible triboelectricnanogenerators: performance improvements and fundamental mechanisms. J. Mater. Chem. A *2*, 13219–13225.

Fan, X., Chen, J., Yang, J., Bai, P., Li, Z., and Wang, Z.L. (2015). Ultrathin, rollable, paper-based triboelectricnanogenerator for acoustic energy harvesting and self-powered sound recording. ACS Nano *9*, 4236–4243.

Han, J.H., Park, K.-I., and Jeong, C.K. (2019). Dual-structured flexible piezoelectric film energy harvesters for effectively integrated performance. Sensors *19*, 1444–1457.

Huang, T., Zhang, Y., He, P., Wang, G., Xia, X., Ding, G.Q., and Tao, T.H. (2020). "Self-Matched"tribo/piezoelectric

nanogenerators using vapor-induced phase-separated poly(vinylidene fluoride) and recombinant spider silk. Adv. Mater. *32*, 1907336.

Jeong, C.K., Hyeon, D.Y., Hwang, G.-T., Lee, G.-J., Lee, M.-K., Park, J.-J., and Park, K.-I. (2019). Nanowire-percolated piezoelectric copolymer-based highly transparent and flexible self-powered sensors. Mater. Chem. A *7*, 25481–25489.

Kanik, M., Say, M.G., Daglar, B., Yavuz, A.F., Dolas, M.H., El-Ashry, M.M., and Bayindir, M. (2015). A motion- and sound-activated, 3D-printed, chalcogenide-based triboelectricnanogenerator. Adv. Mater. *27*, 2367–2376.

Kim, H.S., Kim, D.Y., Kim, J.-E., Kim, J.H., Kong, D.S., Murillo, G., Lee, G.-H., Park, J.Y., and Jung, J.H. (2019). Ferroelectric-polymer-enabled contactless electric power generation in triboelectricnanogenerators. Adv. Funct. Mater. *29*, 1905816.

Lapčinskis, L., Mālnieks, K., Blūms, J., Knite, M., Oras, S., Käämbre, T., Vlassov, S., Antsov, M., Timusk, M., and Šutka, A. (2019). The adhesion-enhanced contact electrification and efficiency of triboelectricnanogenerators. Macromol.Mater.Eng. *305*, 1900638.

Lapčinskis, L., Mālnieks, K., Linarts, A., Blūms, J., Šmits, K., Järvekülg, M., Knite, M., and Sutka, A. (2019). Hybrid tribo-piezo-electric nanogenerator with unprecedented performance based on ferroelectric composite contacting layers. ACS Appl. Energy Mater. *2*, 4027–4032.

Lee, K.Y., Kim, S.K., Lee, J.-H., Seol, D., Gupta, M.K., Kim, Y., and Kim, S.W. (2016). Controllable charge transfer by ferroelectric polarization mediated triboelectricity. Adv. Funct. Mater. *26*, 3067–3073.

Lee, B.-Y., Kim, D.H., Park, J., Park, K.-I., Lee, K.J., and Jeong, C.K. (2019). Modulation of surface physics and chemistry in triboelectric energy harvesting technologies. Sci. Technol. Adv. Mater. *20*, 758–773.

Seung, W., Yoon, H.-J., Kim, T.Y., Ryu, H., Kim, J., Lee, J.-H., Kim, S., Park, Y.K., Park, Y.J., and Kim, S.-W. (2017). Boosting power-generating performance of triboelectricnanogenerators via artificial control of ferroelectric polarization and dielectric properties. Adv. Energy Mater. *7*, 1600988.

Suo, G., Yu, Y., Zhang, Z., Wang, S., Zhao, P., Li, J., and Wang, X. (2016). Piezoelectric and triboelectric dual effects in mechanical-energy harvesting using $BaTiO_3$/polydimethylsiloxane composite film. ACS Appl. Mater. Interfaces *8*, 34335–34341.

Šutka, A., Mālnieks, K., Linarts, A., Timusk, M., Jurķāns, V., Gorņevs, I., Blūms, J., Bērziņa, A., Joost, U., and Knite, M. (2018). Inversely polarised ferroelectric polymer contact electrodes for triboelectric-like generators from identical materials. Energy Environ. Sci. *11*, 1437–1443.

Šutka, A., Linarts, A., Mālnieks, K., Stiprais, K., and Lapčinskis, L. (2019). Dramatic increase in polymer triboelectrification by transition from a glassy to rubbery state. Mater.Horiz. https://doi.org/10.1039/C9MH01425J.

Šutka, A., Malnieks, K., Lapčinskis, L., Kaufelde, P., Linarts, A., Berziņa, A., Zabels, R., Jurķans, V., Gorņevs, I., Blums, J., and Knite, M. (2019). The role of intermolecular forces in contact electrification on polymer surfaces and triboelectricnanogenerators. Energy Environ. Sci. *12*, 2417–2421.

Wang, S., Zi, Y., Zhou, Y.S., Li, S., Fan, F., Lin, L., and Wang, Z.L. (2016). Molecular surface functionalization to enhance the power output of triboelectricnanogenerators. J. Mater. Chem. A *4*, 3728–3734.

Yang, X., and Daoud, W.A. (2017). Synergetic effects in composite-based flexible hybrid mechanical energy harvesting generator. J. Mater. Chem. A *5*, 9113–9121.

Yao, G., Kang, L., Li, J., Long, Y., Wei, H., Ferreira, C.A., Jeffery, J.J., Lin, Y., Cai, W., and Wang, X. (2018). Effective weight control via an implanted self-powered vagus nerve stimulation device. Nat. Commun. *9*, 5349.

Yun, B.K., Kim, J.W., Kim, H.S., Jung, K.W., Yi, Y., Jeong, M.-S., Ko, J.-H., and Jung, J.H. (2015). Base-treated polydimethylsiloxane surfaces as enhanced triboelectricnanogenerators. Nano Energy *15*, 523–529.

Zhang, L., Zhang, B., Chen, J., Jin, L., Deng, W., Tang, J., Zhang, H., Pan, H., Zhu, M., Yang, W., and Wang, Z.L. (2015). Lawn structured triboelectricnanogenerators for scavenging sweeping wind energy on rooftops. Adv. Mater. *28*, 1650–1656.

Zhang, Y., Sun, H., and Jeong, C.K. (2018). Biomimetic Poriferaskeletal structure of lead-free piezocomposite energy harvesters. ACS Appl. Mater. Interfaces *10*, 35539–35546.

Zheng, Y., Cheng, L., Yuan, M., Wang, Z., Zhang, L., Qin, Y., and Jing, T. (2014). An electrospun nanowire-based triboelectricnanogenerator and its application in a fully self-powered UV detector. Nanoscale *6*, 7842–7846.

Zhou, T., Zhang, C., Han, C.B., Fan, F.R., Tang, W., and Wang, Z.L. (2014). Woven structured triboelectricnanogenerator for wearable devices. ACS Appl. Mater. Interfaces *6*, 14695–14701.

iScience, Volume *23*

Supplemental Information

Matching the Directions of Electric Fields from Triboelectric and Ferroelectric Charges in Nanogenerator Devices for Boosted Performance

Andris Šutka, Kaspars Mālnieks, Linards Lapčinskis, Martin Timusk, Kaspars Pudzs, and Martins Rutkis

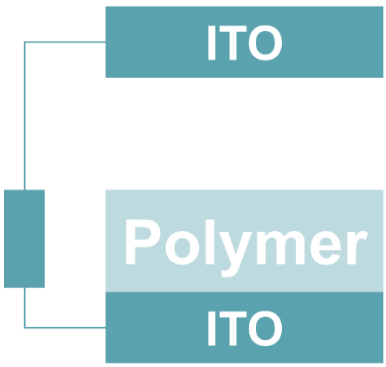

Figure S1, related to Figure 1 (a). Simplified schematic TENG device.

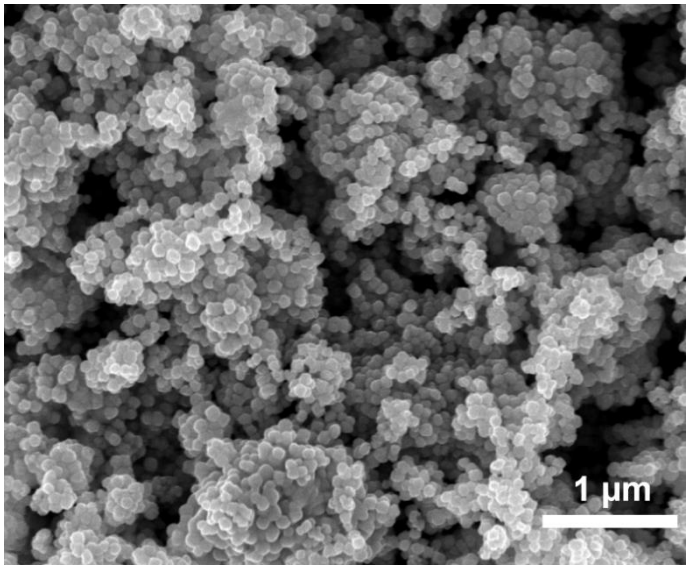

Figure S2, related to Figure 1 (a). SEM image of commercial $BaTiO_3$ nanoparticles (Sigma-Aldrich, CAS number 467634) used for sample film properties.

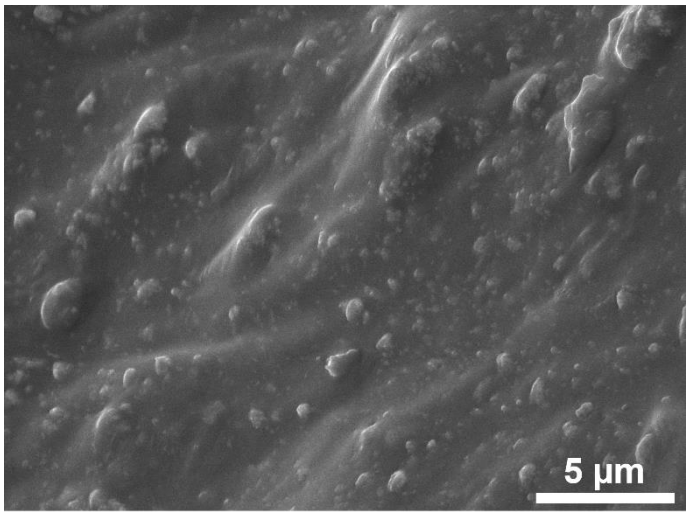

Figure S3, related to Figure 1 (a). SEM image of $BaTiO_3$/PDMS composite film cross-section.

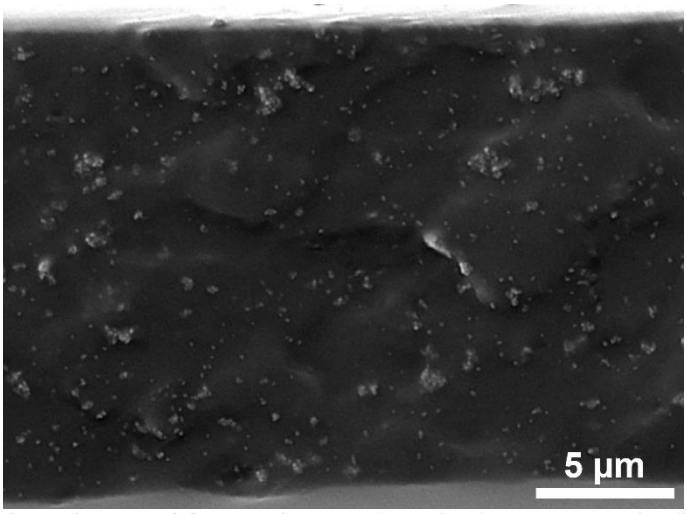

Figure S4, related to Figure 1 (a). SEM image of $BaTiO_3$/EVA composite film cross-section.

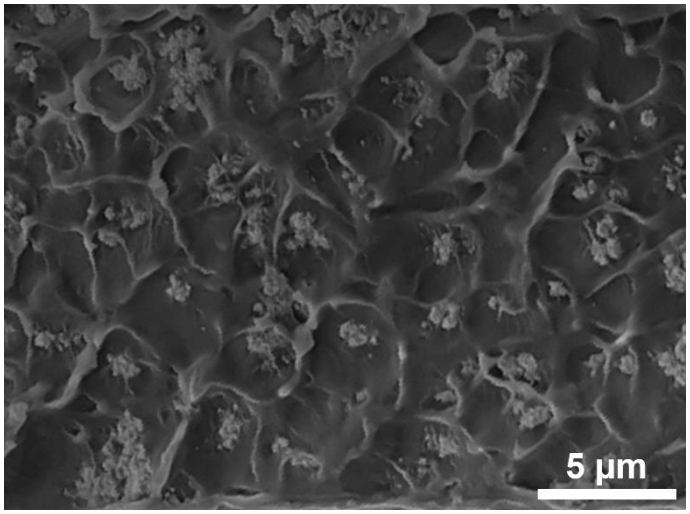

Figure S5, related to Figure 1 (a). SEM image of $BaTiO_3$/PVAc composite film cross-section.

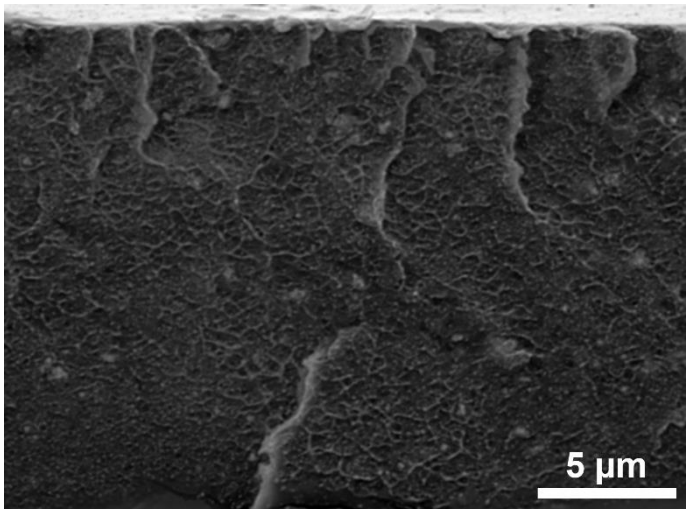

Figure S6, related to Figure 1 (a). SEM image of $BaTiO_3$/PMMA composite film cross-section.

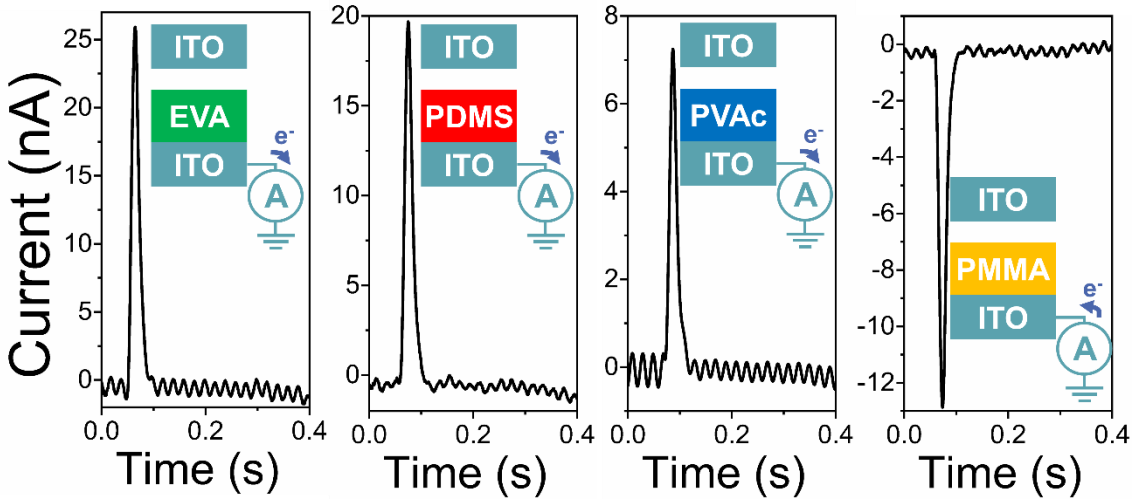

Figure S7, related to Figure 1 (b). Faraday cup regime measurements of EVA, PDMS, PVAc and PMMA against ITO with the corresponding schemes.

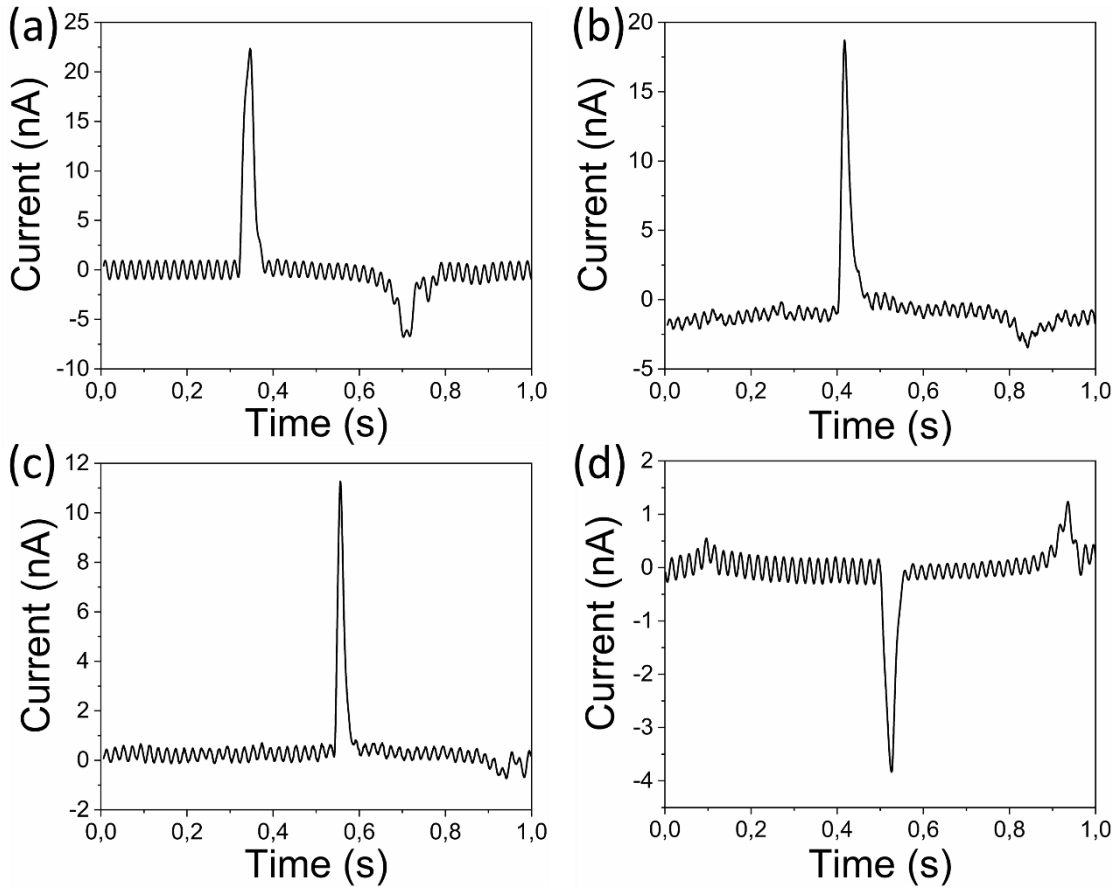

Figure S8, related to Figure 1 (b). Faraday cup regime measurements of (a) $BaTiO_3$/EVA, (b) $BaTiO_3$/PDMS, (c) $BaTiO_3$/PVAc and (d) $BaTiO_3$/PMMA composites against ITO.

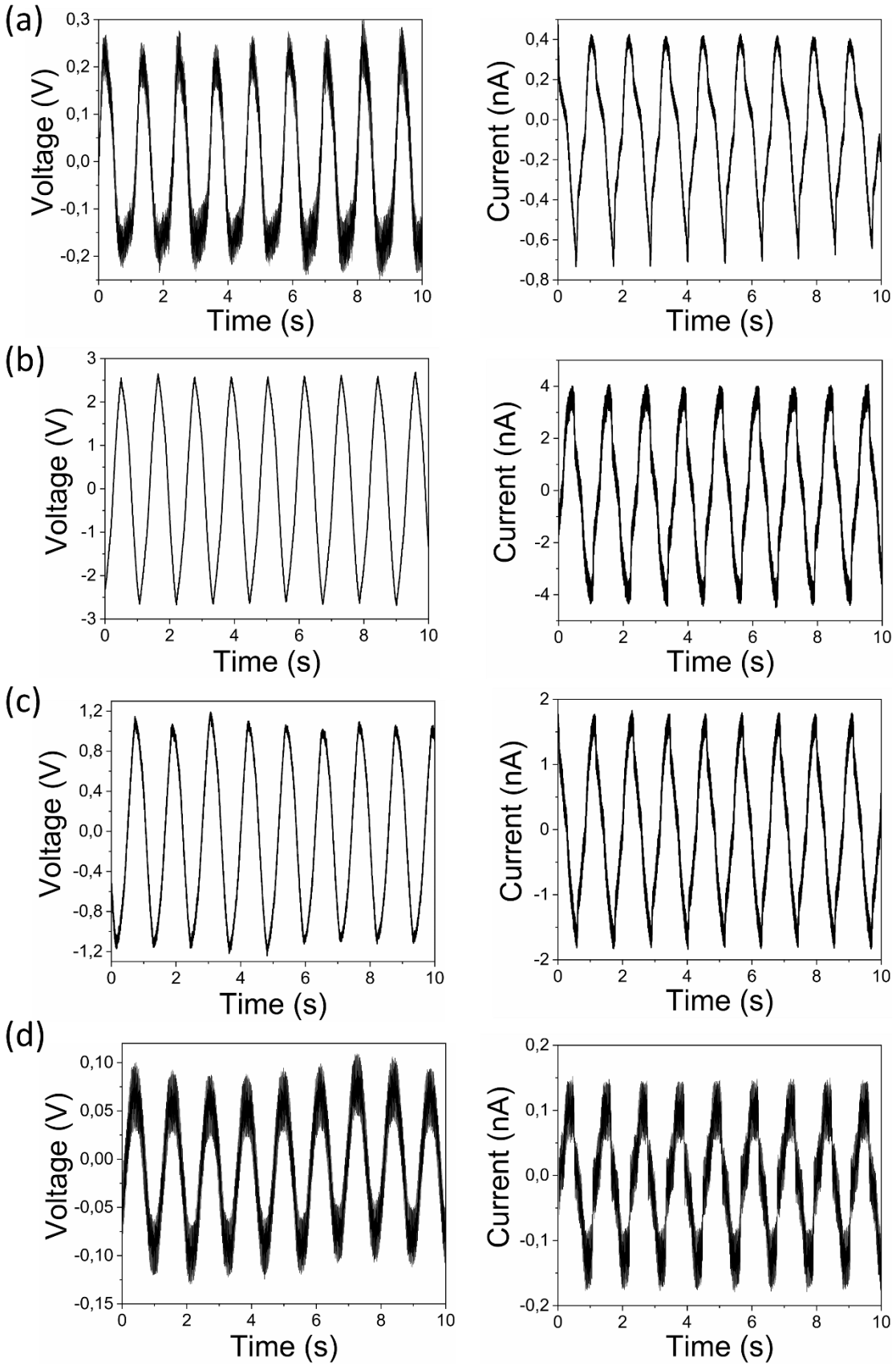

Figure S9, related to Figure 1 (a). Piezoelectric V_{OC} and I_{SC} of (a) $BaTiO_3$/EVA, (b) $BaTiO_3$/PDMS, (c) $BaTiO_3$/PVAc and (d) $BaTiO_3$/PMMA composites.

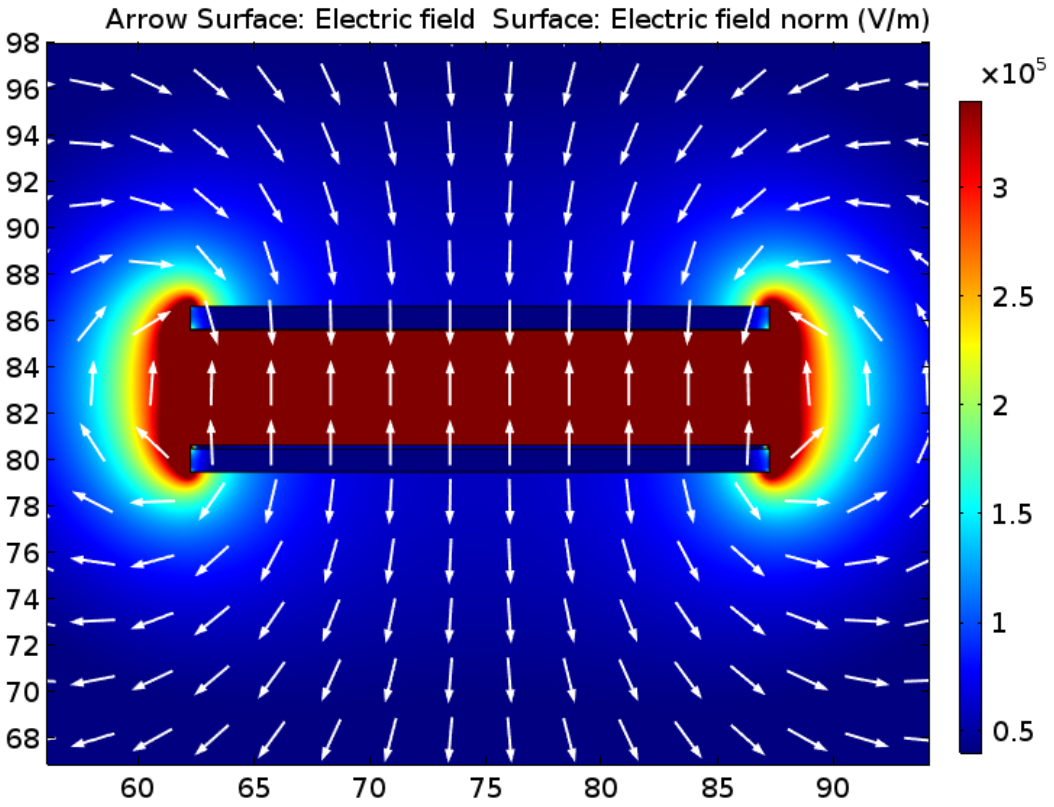

Figure S10, related to Figure 2. COMSOL finite element simulation of contact-separation between two films. The dipole formed between PDMS and opposite layer is shown in the middle where the highest electric field is observed (3.4×10^5 V m^{-1}).

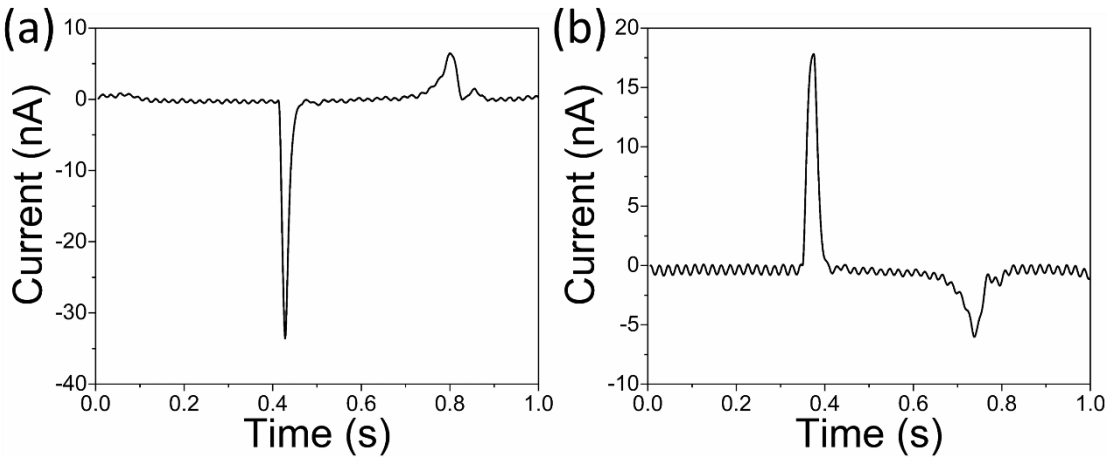

Figure S11, related to Figure 3 (a). Faraday cup regime measurements of (a) PMMA sample contacted with PDMS layer and (b) PDMS sample contacted with PMMA layer.

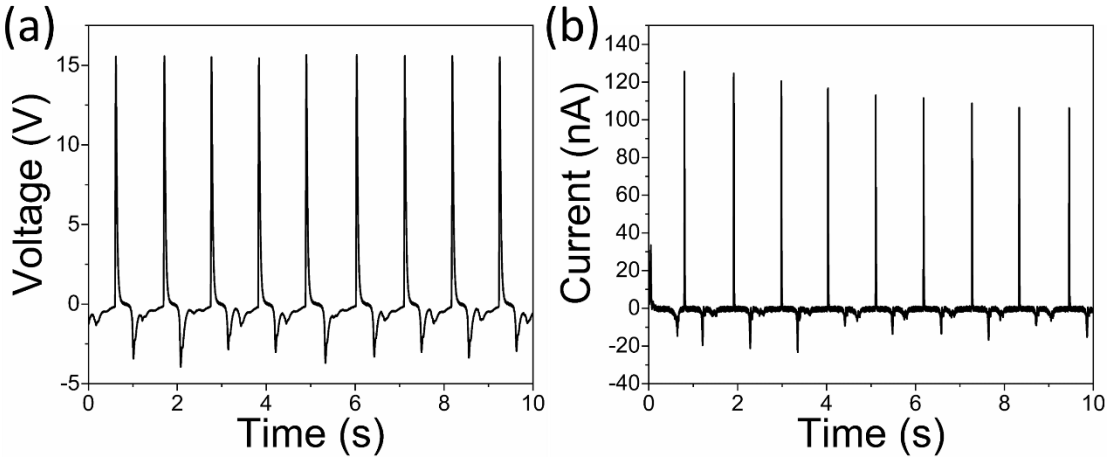

Figure S12, related to Figure 3 (b). (a) V_{OC} and (b) I_{SC} of TENG device constructed from PDMS and PMMA polymers without $BaTiO_3$ NPs.

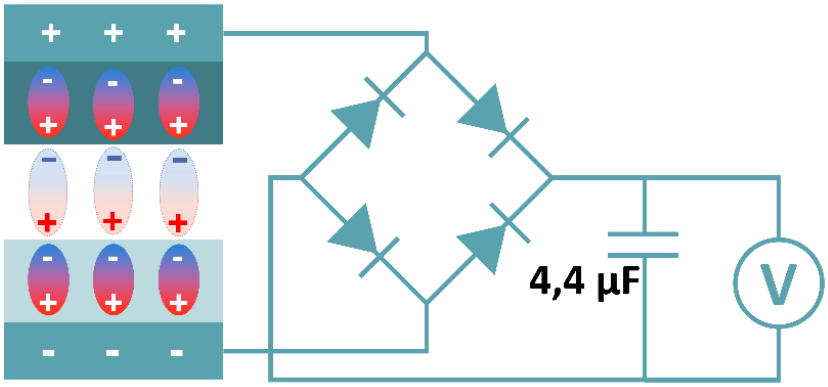

Figure S13, related to Figure 3 (d). Capacitor charging scheme. Alternating current signal from TENG device is rectified and energy is stored in 4.4 µF capacitor. Voltage is measured to determine the charge state of capacitor.

Transparent methods

Polydimethylsiloxane (PDMS), ethylene-vinyl acetate copolymer (EVA), poly(vinyl acetate) (PVAc) and poly(methyl methacrylate) (PMMA) were used in our studies to prepare TENG devices. The polymer film was deposited on indium-tin oxide (ITO) coated polyethylene terephthalate (PET) substrate by spin-coating and contacted with another ITO (see Figure S1 for schematic TENG device representation). Polydimethylsiloxane (PDMS, Sylgard 184 kit) films were prepared by mixing base polymer and curing agent in a 10:1 ratio. PDMS films were spin-coated directly on ITO conductive electrode. The rotation speed was 3000 rpm. Before spin coating, mixture was degassed and PDMS films were cured at 80°C for 30 min. Polymers EVA (Sigma Aldrich, 40 wt% vinyl acetate) and PVAc (Sigma Aldrich, average Mw 100`000) were dissolved in toluene in 20 wt%, while dimethylformamide was used for PMMA (Sigma Aldrich, average Mw 120`000). Solutions were spin-coated onto ITO/PET at 3000 rpm and dried in ambient atmosphere to obtain polymer films. The ferroelectric properties for polymer films were provided by adding 7.5 vol% $BaTiO_3$ nanoparticles <100 nm in size (see Fig. S2 for scanning electron microscopy (SEM) image). Nanoparticles were dispersed in polymer solutions using ultra sonification probe Hielscher UP200S for 3 minutes. The cross-section images for composites are demonstrated in Fig. S3-S6. Polarization of prepared $BaTiO_3$ and polymer composite films was conducted using 20 MV m^{-1} electric field at 90 °C temperature.

The open-circuit voltage (V_{OC}) at load resistance $1 \cdot 10^9$ Ω and short-circuit current (I_{SC}) was measured by using a custom-made voltage divider in combination with a Keithley 6514 electrometer connected to a Picoscope 5444B PC oscilloscope to provide high time resolution. The surface charges were calculated from current measured in Faraday cup regime between TENG electrode and ground (shown in Figure S7) by using equation $Q=\int i dt$ (where i – instantaneous current). Contacting area (sample size) in all tests was 5 cm^2. Pressing force (10 N), frequency (1 Hz), separation speed (10 mm s^{-1}) and gap (5 mm) between sample sides for TENG performance measurements were kept constant by using INSTRON E1000 All-Electric Dynamic Test Instrument. The instantaneous power density was calculated by Joule's Law: $P=V^2R^{-1}$, where V is voltage and R is load resistance. Integration of instantaneous power density over time gives energy density obtained during contact-separation. Next, energy density divided by the duration of the peak results in the average power density. The 4.4 μF capacitor was charged as depicted in Figure S13. Energy stored in this capacitor was calculated by $E=0.5CV^2$ (C is capacitance of capacitor and V is voltage measured across capacitor).

Kelvin probe measurements were performed using Scanning Kelvin Probe system SKP5050. Surface potential of the sample was scanned by oscillating 2 mm tip in 10-by-10 point area (total 100 points) to obtain surface potential maps. Distance between two scanned points was approximately 250 μm, therefore almost the whole area of sample was scanned. Potential maps of non-polarized and polarized (both positively and negatively) $BaTiO_3$/PDMS samples before and after contacting with PMMA polymer is shown in Figure 4 in main text. The contact with PMMA was accomplished by placing this layer on $BaTiO_3$/PDMS sample still in device and applying load of 10 N for 1 minute. Second scan was performed right after the removal of PMMA.

The electric field strength and gradient were simulated for contacting-separating PDMS film with ITO by using COMSOL finite element analysis software. Charge density used for electric field simulations was calculated from measured current in Faraday cup mode by equation $Q=\int i dt$ (where i – instantaneous current). Simulation results are presented in Figure S10.

Institute of Solid State Physics, University of Latvia as the Center of Excellence has received funding from the European Union's Horizon 2020 Framework Programme H2020-WIDESPREAD-01-2016-2017-TeamingPhase2 under grant agreement No. 739508, project CAMART²